University of Sistan and Baluchestan

Challenges in Nano and Micro Scale Science and Technology

Online ISSN: 2821 - 000X

Effect of Stress Concentration Regions on the Performance of Piezoresistive Silicon Beams

Erfan Rezazadeh Kalashami[1] | Reza Ansari[2] | Mohammad Kazem Hassanzadeh-Aghdam[3]

1. Faculty of Mechanical Engineering, University of Guilan, Rasht, Iran
2. Faculty of Mechanical Engineering, University of Guilan, Rasht, Iran
3. Corresponding author, Department of Engineering Science, Faculty of Technology and Engineering, East of Guilan, University of Guilan, Rudsar-Vajargah, Iran. E-mail: mk_hassanzadehaghdam@guilan.ac.ir

Article Info

Article type:
Research Article

Keywords:
Piezoresistance,
Stress concentration region,
Silicon beam,
Finite element method,
Micro-electro-mechanical-system

ABSTRACT

Piezoresistance, which is the change in resistance due to the applied stress, is a phenomenon that has been recognized in silicon. This study analyzes a micro-electro-mechanical-system (MEMS)-based force sensor that is both flexible and highly sensitive, utilizing a piezoresistive sensing mechanism. The design analysis focuses on enhancing the sensitivity of the microcantilever or beams by integrating various combinations of the stress concentration regions (SCRs). For simulation, four-point bending setup is used specifically for analyzing the piezoresistance effect in p-type silicon. The stress distribution in this setup is niform and aligned with the <110> crystal axis. The primary objective of this study is to investigate the impact of different shapes, distances, rotations, and the number of SCRs on the performance of piezoresistive beam. A finite element approach is employed to analyze different designs for obtaining relative resistance changes. The simulation results are compared with experimental data, demonstrating a good accuracy and it is also identified the appropriate element size for converging answers. As a result, a force sensor has been designed with high sensitivity and flexibility.

1. INTRODUCTION

Beam structures such as microcantilevers are fundamental components in micro-electro-mechanical-systems (MEMS) and find applications in various sensing equipment. These miniature structures, resembling tiny diving boards, exhibit remarkable sensitivity due to their large surface area-to-volume ratio. Among the diverse types of beam structures, silicon microcantilevers stand out as versatile sensors for real-time detection in MEMS devices [1-4].

There are various mechanisms to choose from when designing sensors, but the microcantilever mechanism is preferred for force sensing due to its flexibility, versatility, high sensitivity, and cost-effectiveness [5]. There are several types of sensing mechanisms available for microscale sensing, such as piezoelectric, capacitive, and piezoresistive. However, when it comes to force sensing, the piezoresistive sensing mechanism is often the preferred choice due to its compact size, excellent resolution, minimal phase lag, low cost, superior sensitivity, wide dynamic range, straightforward manufacturing process, and seamless integration capabilities [6].

Micro-beams used in MEMS are typically composed of silicon or silicon derivatives. These structures are widely used in atomic force microscopy (AFM), microcantilevers enable topographic imaging of non-conductive surfaces [7]. Over the past decade, they have been evolved into powerful transduction platforms for chemical, biological, and physical sensing applications. Piezoresistive sensors exploit changes in electrical resistance due to mechanical strain. When a force or stress is applied to a piezoresistor, its resistance changes proportionally. Piezoresistive silicon microcantilevers utilize this principle for sensing various parameters [8].

The design of the structure of this type of sensors considers making the right choices in dimensions, stiffness constant, and resonant frequency to meet specific measurement requirements. When dealing with simple rectangular cantilevers, there are established mathematical expressions for determining these parameters [9]. However, when dealing with more complex structures, finite element modeling becomes valuable for analyzing and improving the structural design. Additionally, the method used for detecting the deflections of the cantilever

How to Cite this paper: Rezazadeh Kalashami E. Ansari R. Hassanzadeh-Aghdam M.K. Effect of Stress Concentration Regions on the Performance of Piezoresistive Silicon Beams. *Challenges in Nano and Micro Scale Science and Technology*. 2024; 12(2): 41-57. DOI: 10.22111/cnmst.2025.52964.1267

DOI: 10.22111/cnmst.2025.52964.1267

is crucial. Piezoresistive detection is highly desirable as it eliminates the need for lasers and complex optics, and it also allows for the potential of operating multiple cantilevers simultaneously [6,10]. There is a significant interest in enhancing the sensitivity of force and displacement detection, as this would enable more precise measurements of smaller deflections [11].

To investigate the piezoresistance effect, researchers should assess the relative change in electrical resistance when subjected to the mechanical stress. This entails precise application of both electric fields and mechanical stress along the controlled crystallographic directions [12-14]. These conditions must be maintained across varying temperatures and stress levels. Various setups have been employed, including membranes, cantilevers, and beams, each subjected to different loading configurations. Four-point bending (4PB) method for mechanical loading is a technique involving bending a silicon beam, supported at two points, by applying a force at two other points. Notably, this well-established method ensures uniform stress distribution along the beam, determined by sample geometry, support position, load placement, and load magnitude. Furthermore, it exhibits robustness against minor alignment errors. In the realm of microfabrication, particularly when dealing with thin film devices, the use of a 4PB fixture is often deemed more advantageous. This is primarily due to its ability to provide a more controlled and precise application of stress, which is crucial in the manipulation and testing of these delicate devices [12-14].

In the studies referenced as [12,13,15], an optical method was employed to measure the deflection and curvature of the chip. This method involves the use of light to accurately measure the physical changes in the chip when subjected to the stress. The stress, in these cases, was applied to the chip using a piezoelectric actuator and a translation stage, respectively. These tools allow for a precise and controlled application of stress, which is crucial in obtaining accurate measurements. In Ref. [16], the displacement of the chip was known at the contact points between the chip and the 4PB fixture. This knowledge of displacement at specific points allows for a calculation of the applied stress in the chip. Understanding the stress distribution within the chip is crucial in predicting its behavior under different loading conditions. In Refs. [13,17], simple loads were used to apply the force. However, some studies did not include an external measurement of the applied force. This lack of external force measurement can lead to uncertainties in the results. Also, temperature can significantly affect the properties of the chip, and therefore, characterizing it at different temperatures is crucial in understanding its behavior under various conditions.

A novel technique aimed at amplifying the surface stress of a structure is by incorporating stress concentration holes into the design of simple beams, which are typically used for sensing small forces and put it under bending to measure relative resistance change. The primary function of these holes is to localize the stresses experienced by the device. Firdaus et al. [10] conducted an analysis comparing earlier studies on piezoresistive microcantilevers, both with and without SCR. They found that the inclusion of a rectangular SCR enhances the device's sensitivity. Wahid et al. [18] also performed simulations and observed that a cantilever equipped with a circular SCR exhibited a greater extent and a wider region of stress distribution, which markedly enhances the piezoresistive effect. Ref. [11] showed the enhancement of micro piezoresistive cantilevers by optimizing their mechanical and electrical design parameters. By doing so, the sensitivity of these devices increases significantly. Also, a finite element method (FEM)-based simulation is employed to identify the optimal location for the piezoresistor. Additionally, introducing specific structural discontinuities in the cantilevers enhanced the sensitivity. All of these studies and other literatures mostly analyzed and observed the stress distribution and deflection in microcantilevers [18].

Current study utilizes a commercial finite element analysis software to investigate the enhancement of piezoresistive sensitivity that is resulted from the use of the stress concentration holes. We examined many fundamental designs in this study. These designs were all variations of simple type silicon beam, each featuring different patterns of holes. P-type doped silicon, widely used in piezoresistive MEMS due to its large π_{44} coefficient and favorable piezoresistive properties, was selected as the material for the beams in this study. This well-established preference is due to the large value of the piezoresistive coefficient π_{44} in p-type doped silicon, coupled with the extremely low values of the other two piezoresistive coefficients, π_{11} and π_{12}.

2. Principle of piezoresistive force sensor and formulation

The theoretical framework of the piezoresistive phenomenon is intimately intertwined with the conductive properties inherent to the semiconductor material under consideration. This intimate relationship is a direct consequence of the fundamental principles governing the behavior of semiconductors.

In light of this, the principle underlying the piezoresistive effect implies that the term involving (Σ), which represents the electric field, can be depicted using the subsequent mathematical formulation. The formulation below (Eq. 1) is crucial as it encapsulates the relationship between the piezoresistive effect and the electric field, providing a comprehensive understanding of how changes in the electric field can influence the piezoresistive properties of the semiconductor. This, in turn, can have significant implications in various applications where piezoresistive materials are used [8].

$$\Sigma = \rho \cdot J + \Delta\rho \cdot J \tag{1}$$

Here, (J) denotes the current, (ρ) represents the resistivity, and ($\Delta\rho$) corresponds to the change in resistivity resulting from the applied stress. The relative change in resistivity is defined as [8]:

$$\Delta\rho = \pi \cdot \sigma \tag{2}$$

In this context, (π) represents the tensor of piezoresistance, which has units of Pa^{-1}, and (σ)

symbolizes the stress. Essentially, the proportional relationship between the relative alterations in resistivity and resistance is established. Consequently, the variation in resistance for a the piezoresistor response can be expressed as a function of both longitudinal and transverse stresses, as illustrated in the following formulation [12,13,17,19]

$$\frac{\Delta\rho}{\rho} = \frac{\Delta R}{R} = \pi_l \cdot \sigma_l + \pi_t \cdot \sigma_t \tag{3}$$

The piezoresistive coefficients are represented by (σ_l) and (σ_t), which correspond to the longitudinal and transverse stress, respectively. Given that 4PB results in uniaxial stress, Since the stress is predominantly in the longitudinal direction, the transverse stress component can be neglected in this equation. This leads to the following simplified form [12,13,17,19]

$$\frac{\Delta R}{R} \cong \pi_l \cdot \sigma_l \tag{4}$$

π_l which is the coefficient of effective piezoresistivity, can be ascertained by gauging the fundamental piezoresistive coefficients in silicon, namely (π_{11}), (π_{12}), and (π_{44}). When a stress is applied uniaxially in p-type silicon, along the <110> direction, the equation can be further streamlined to the following form [12,13,17,19]

$$\pi_l = \frac{1}{2}(\pi_{11} + \pi_{12} + \pi_{44}) \tag{5}$$

Table 1
Room-temperature piezoresistive coefficients for silicon at 10^{-11}Pa^{-1}[8].

Resistivity	$\boldsymbol{\pi_{11}}$	$\boldsymbol{\pi_{12}}$	$\boldsymbol{\pi_{44}}$
7.8Ω-cm. p-type	6.6	-1.1	138.1

Table 1 showcases the standard piezoresistive coefficients for lightly doped silicon. It is clear that the value of π_{44} significantly surpasses those of π_{11} and π_{12}, thus, they can be overlooked as inferred in the preceding equation (Eq. 5)

The equation that shows the relationship between the piezoresistive coefficient, denoted as $\pi(N,T)$ and dependent on impurity concentration (N) and temperature (T) can be formulated as follows. This equation allows us to understand how changes in the impurity concentration and temperature can influence the piezoresistive coefficient [12,13,17,19].

$$\pi(N.T) = P(N.T) \cdot \pi(300°K) \tag{6}$$

In this context, $P(N,T)$ represents the piezoresistance factor, a key element in this analysis. For the purpose of this study, we utilize a 4PB setup. The simgulation of the piezoresistive beam is based on the linear elastic theory for mechanical deformation:

$$\sigma = \mathbf{C}:\epsilon \tag{7}$$

where σ is the stress tensor, ϵ is the strain tensor, and $\mathbf{C}$ is the stiffness tensor of p-type silicon along the <110> crystallographic direction.

The stress at the center of the beam, denoted as (σ_c), is of particular interest. The value of σ_c can be accurately calculated using the following equation. This equation allows us to quantify the stress experienced by the silicon beam under the conditions created by the 4PB setup [20].

$$\sigma_c = \frac{3Fa}{wt^2} \tag{8}$$

In this equation, (F) represents the applied force, a stands for the distance between the supports, (w) denotes the beam's width, and (t) signifies the beam's thickness. The eflection at the loading point, denoted by (z), can be calculated as follows [20]

$$z = \frac{(12aL - 16a^2)aF}{4Et^3w} \tag{9}$$

In this formula, the symbol (L) represents the length between the external supports, while (E) stands for the elastic modulus of the substance which is silicon. In the finite element simulations, the beam was modeled with the 4PB boundary conditions described above, with the outer supports constrained in the vertical direction and inner loading points applying forces to produce a uniform bending moment in the central region. Perfect contact was assumed at supports and loading points. The coupled mechanical and electrical problem was solved using the piezoresistive formulations (Eqs. 1-7), with mesh convergence ensured to achieve numerical accuracy. The simulations assume homogeneous, anisotropic silicon properties along <110> direction, linear elastic deformation, and linear piezoresistive response. Validation was performed against experimental and analytical data to confirm the model's accuracy. The equations for both stress and deflection are applicable in this scenario. However, it's important to note that these equations are predicated on the assumption that the deformation or bending of the beam is relatively small. If the deformation was large, the equations might not hold true, and other factors could come into play, potentially requiring a more complex analysis. This is a common assumption in many engineering applications where the deformations are indeed usually small enough that the linear equations are a good approximation.

3. MATERIALS SELECTION

The properties of the materials used in the design and simulation of force sensors are a crucial factor that must be taken into account. In this particular investigation, the mechanical properties of silicon are considered for the design of the structure because one of the most commonly used substrate materials in the realm of MEMS technology is silicon. This is largely due to its highly sensitive mechanical properties which enable it to produce a large displacement in response to forces in the micro-Newton range, which are relatively low.

To convert this displacement into a measurable voltage, a material with piezoresistive properties is employed. In this case, the material of choice is p-type Silicon, due to its inherent piezoresistive properties. For the purpose of connecting the piezoresistors, thin layers of

gold are utilized. Gold is chosen for its excellent electrical conductivity and resistance to oxidation.

Finally, some of the key properties of the materials used, such as electrical conductivity, relative permittivity, density, and modulus of elasticity, are listed in Table 2 [21-23]. These properties are essential for understanding the behavior of the materials under different conditions and for improving the design and performance of the MEMS Force sensor.

Table 2
Mechanical and geometric properties of piezoresistor and structure [21-23]

Material	$E\ (GPa)$	υ	$D(\frac{kg}{m^3})$	ε_r	$d\ (\mu m)$	$l\ (\mu m)$	$t_i\ (\mu m)$
Silicon	170	0.28	2329	-	6000	40000	400
p-type Silicon	170	0.28	2330	4.5	20	500	1
Gold	57	0.35	19300	1	20	500	1

4. MODEL DEFINITION

The use of a hard piezoresistive material placed on a softer substrate material is a well-established strategy to enhance sensor sensitivity. This approach exploits SCRs, which are geometric features where stress tends to accumulate. SCRs provide an effective means of increasing sensitivity without requiring major structural modifications [18,19,24].

In the present study the focus is on the simulation of piezoresistive silicon beams for sensing and detection applications under 4PB conditions. To enhance stress, displacement, electrical sensitivity, reliability, and flexibility, different SCR geometries were incorporated into the beam design.

In the numerical model, idealized conditions were applied to isolate the influence of SCR geometry on the piezoresistive response. Perfect contact between the beam and the loading/support lines was assumed, as contact deformation has negligible influence on the uniform stress region in 4PB [13]. Material properties of p-type silicon were considered homogeneous and anisotropic along the <110> crystallographic direction, consistent with standard MEMS-grade wafers [12,13,17,19]. Noise sources and temperature effects were excluded to focus solely on the intrinsic stress–resistance relationship.

4.1. Geometry and SCR Configurations

The beam structure includes SCRs of various shapes and sizes, with dimensions summarized in Table 3. The piezoresistors are positioned on the upper surface of the beam where the maximum longitudinal stress occurs. The baseline beam without SCRs serves as the reference model, while other configurations include square, rectangular, circular, hexagonal, and triangular SCRs.

Table 3
SCR dimensions (area of all shapes is 2.25 μm^2)

Shape	$a\ (\mu m)$	$b\ (\mu m)$	$r(\mu m)$
Square	1.5	1.5	-
Rectangular	2.25	1	-
Circular	-	-	0.8465
Hexagonal	-	-	0.9306
Triangular	1.61185	1.3959	0.239
2 Square	1.06066	1.06066	-
4 Square	0.75	0.75	-
2 Circles	-	-	0.5984
4 Circles	-	-	0.423142
2 Hexagons	-	-	0.65802
4 Hexagons	-	-	0.4653
2 Triangles	1.13975	0.9870	-
4 Triangles	0.8060	0.6980	-

Each SCR geometry is studied in multiple arrangements: duplicated twice or four times, rotated at various angles (15°, 30°, 45°, 60°, and 90° as appropriate), and positioned at different distances (1 µm, 1.5 µm, and 2 µm) from the resistor. These variations allow systematic evaluation of the influence of shape, orientation, and proximity on piezoresistive performance. Figures 1(a–f) illustrate the beam geometries and deformation patterns.

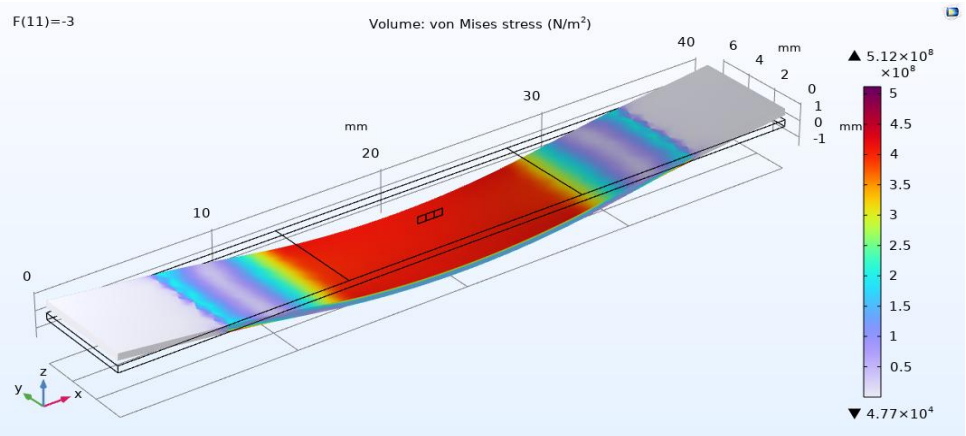

(a)

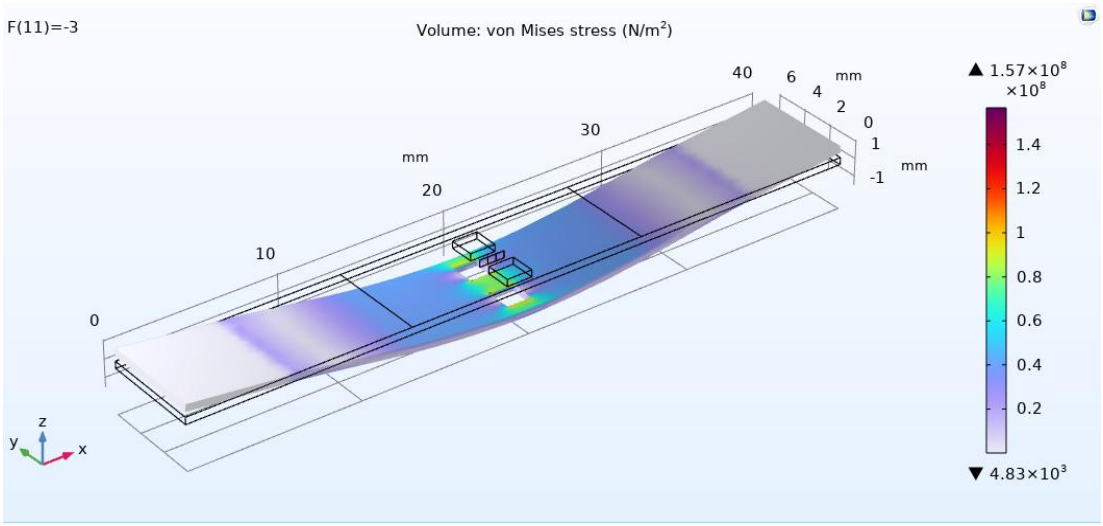
F(11)=-3
Volume: von Mises stress (N/m²)
▲ 1.57×10⁸
×10⁸
1.4
1.2
1
0.8
0.6
0.4
0.2
▼ 4.83×10³
mm
40
30
20
10
0
6
4
2
0
1
-1
z
y
x

(b)

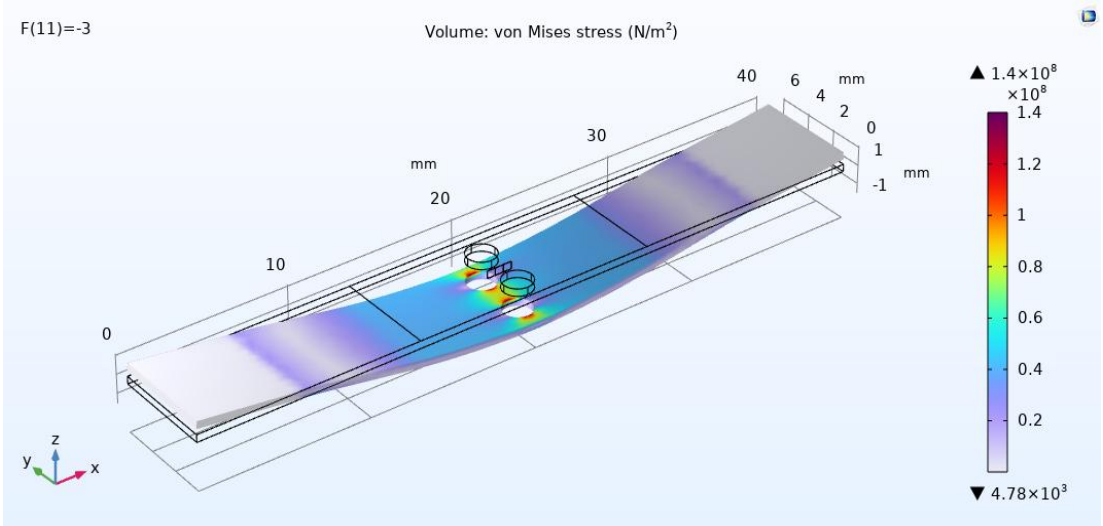
F(11)=-3
Volume: von Mises stress (N/m²)
▲ 1.4×10⁸
×10⁸
1.4
1.2
1
0.8
0.6
0.4
0.2
▼ 4.78×10³
mm
40
30
20
10
0
6
4
2
0
1
-1
z
y
x

(c)

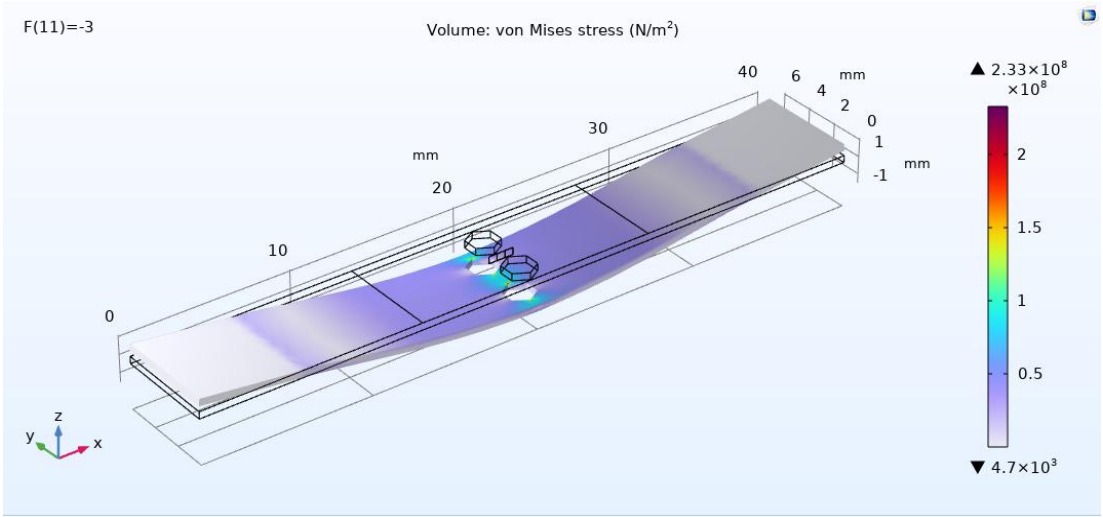
F(11)=-3
Volume: von Mises stress (N/m²)
▲ 2.33×10⁸
×10⁸
2
1.5
1
0.5
▼ 4.7×10³
mm
40
30
20
10
0
6
4
2
0
1
-1
z
y
x

(d)

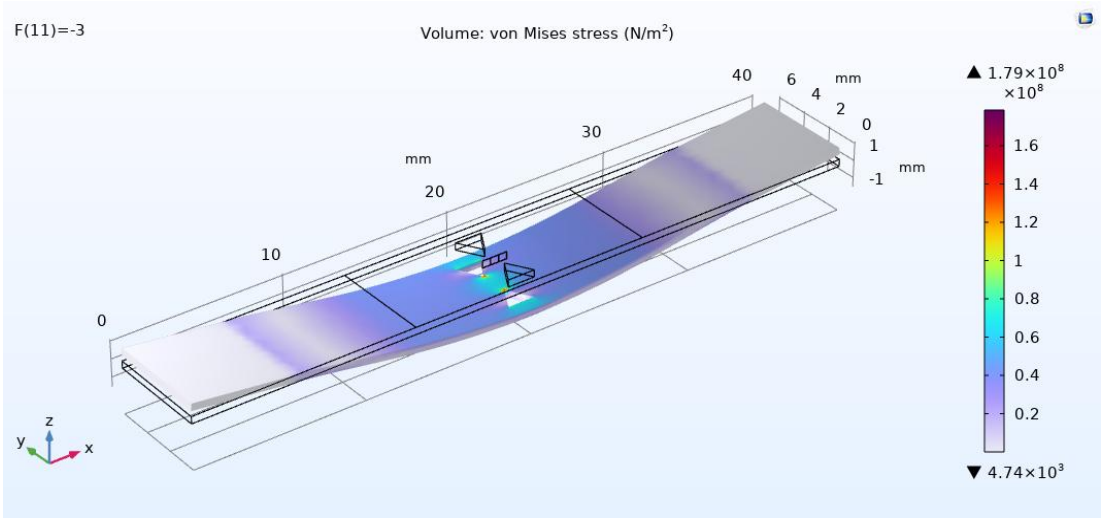

(e)

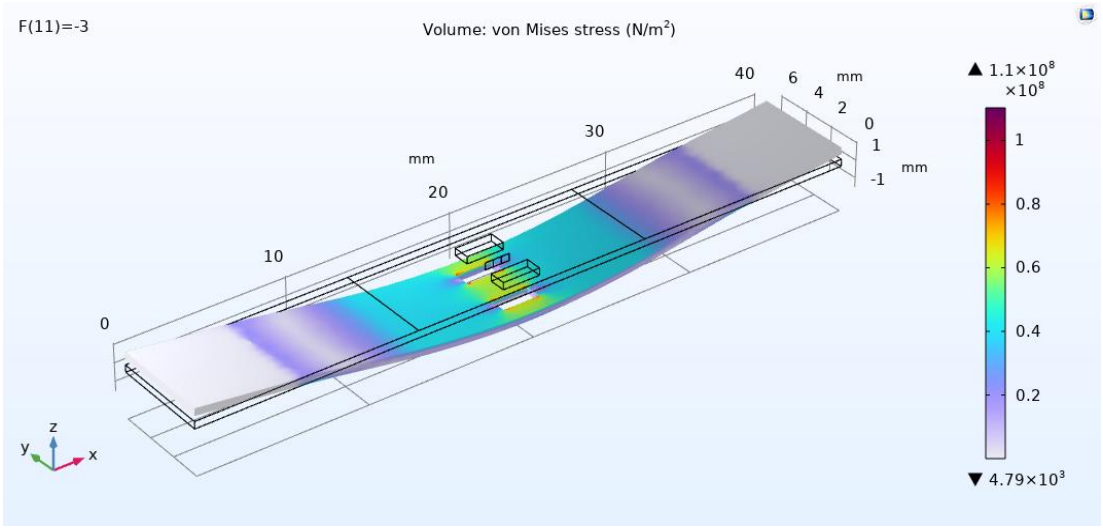

(f)

Fig. 1. Silicon beam models (a) without SCRs and with (b) square, (c) circular, (d) hexagonal, (e) triangular and (f) rectangular SCRs.

4.2. Simulation Configuration

The 3D model under consideration is solely comprised of a silicon beam, as illustrated in Fig. 2. The silicon beam's dimensions are specified as 40 mm in length, 6 mm in width, and 400 μm in thickness. The properties of the silicon used in this simulation are detailed in Table 2. As depicted in Fig. 3, there are two lines, one inner and one outer, distanced at 14 mm and 28 mm respectively. These lines exert the loading forces and impose restrictions on the silicon beam. Herein, 4PB was used to apply load to the test beams. The bending moment between the two inner load lines is constant, producing a nearly uniform bending stress and negligible moment gradient within the central region of the beam; this enables direct correlation between applied mechanical stress and the measured piezoresistive response. For material and sensor characterization this is advantageous compared with point loading, which introduces localized stress concentrations and steep stress gradients, or wide area distributed loading, which smooths peak stresses and reduces sensitivity to local geometric stress amplifications. Consequently, the four-point configuration allows controlled application of uniaxial stress in the central test region, facilitating accurate comparison between finite-element simulations and measured $\Delta R/R$ values [13, 25-30].

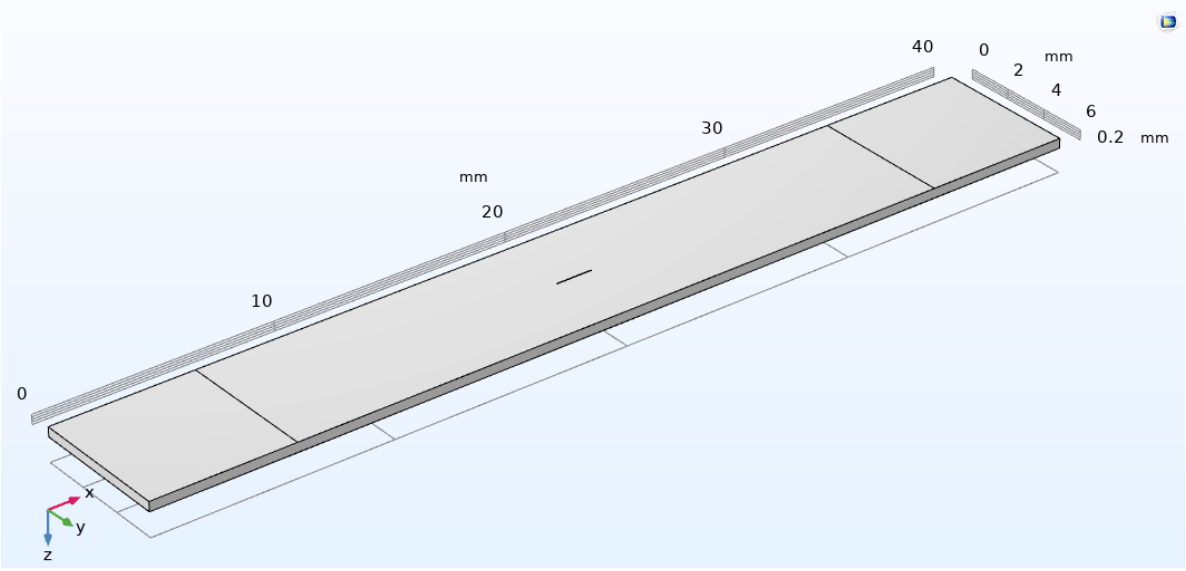

Fig. 2. 3D model of the silicon beam geometry (bottom view) showing overall dimensions and structure used in the simulation.

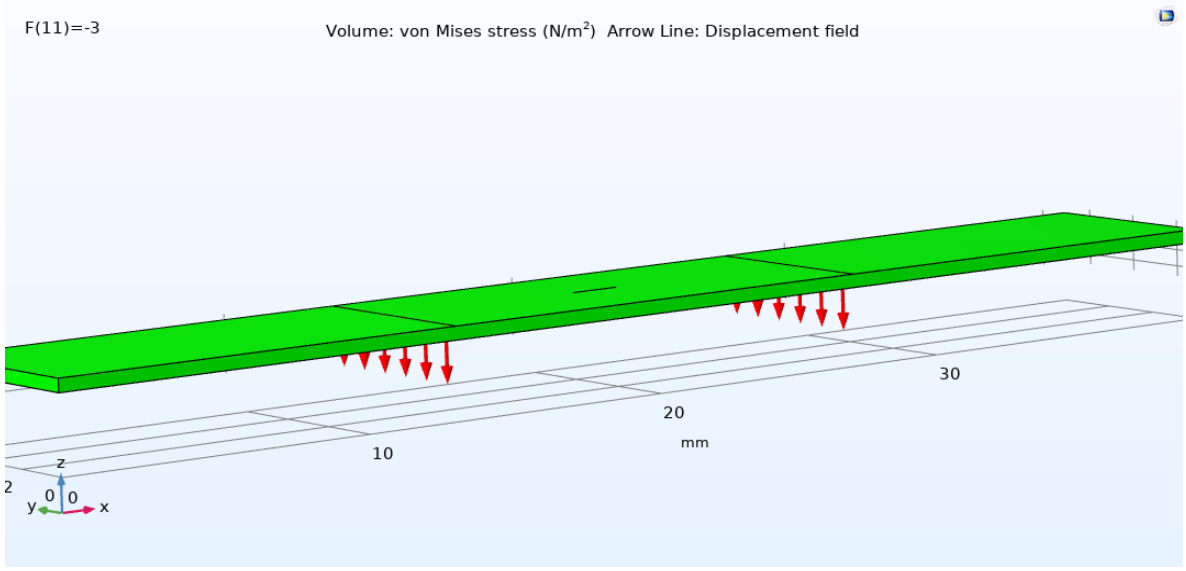

Fig. 3. Schematic of the four-point bending configuration illustrating the applied loading forces on the two inner lines and the corresponding support lines.

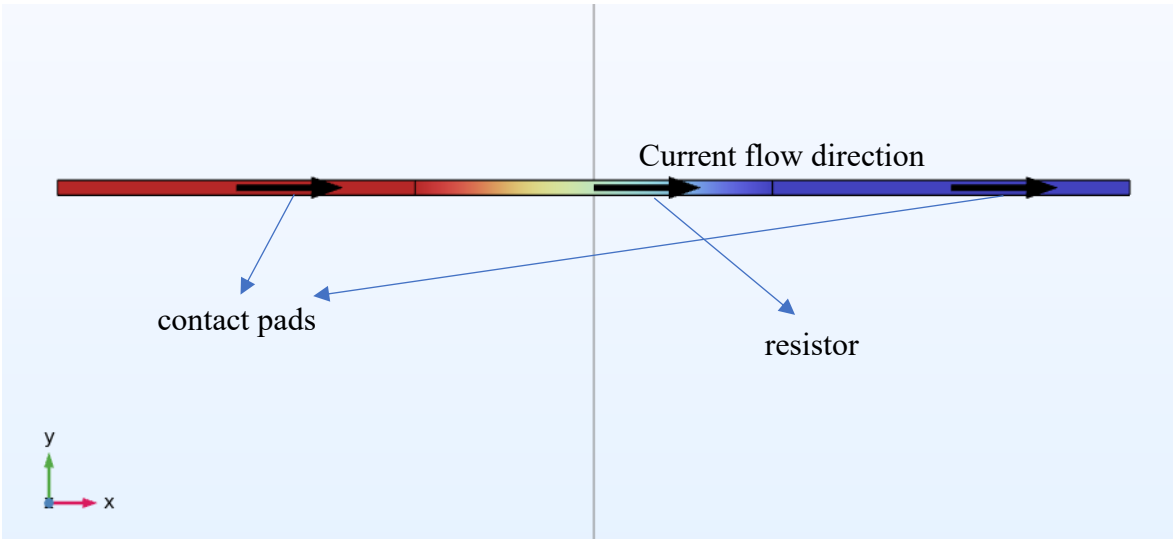

Fig. 4. A two-terminal configuration resistor

As shown in Fig. 4, a rectangular area, situated at the center of the silicon beam, is specifically allocated for the positioning of the piezoresistors. The piezoresistive effect interface has been selected for this simulation allowing for the exploration of piezoresistivity in semiconductor materials. For this specific method, we have coupled solid mechanics and electric currents in single layer shells physics.

In order to study the piezoresistive effect, a configuration of a resistor with two terminals, having dimensions of 500 µm in 20 µm, is integrated into the model. This setup facilitates the measurement of alteration in resistance due to eposed forces on the silicon beam. The terminal piezoresistor is designed with two contact pads that are of similar dimensions. The integration of a thin conductive layer is essential in the development of a piezoresistive model. This is to guarantee a steady flow of conductivity current through the material, which is a critical aspect in accurately capturing the piezoresistive effect.

4.3. Electrical Setup and Boundary Conditions

A 3 V potential difference was applied across the resistor terminals — one connected to the voltage source and the other grounded — ensuring compatibility with typical MEMS operation and avoiding thermal effects [6,19]. Previous studies have established that the FEM is an effective approach for simulating these types of problems [25-29]. In the present study, we make use of a FEM software which allows us to conduct a thorough examination of both the mechanical and electrical behaviors of the sensors.

The resistor thickness is 1 µm, with a doping concentration of $1 \times 10^{19} cm^{-3}$ [19], and the contact pads are doped to $1.5 \times 10^{20} cm^{-3}$[19]. The resistor orientation was aligned along the <110> direction by adjusting the global coordinate system accordingly.

5. RESULTS AND DISCUSSION

The results are divided into three sections for presentation and discussion. First section presents the validation of our results with existing literature, followed by a mesh sensitivity analysis to determine the convergence point. We then compare and analyze the effects of varying the shape, distance, rotation and number of stress concentration regions.

In the simulation, a force pointing downward acts on the beam and the displacement and stress that result from it are measured. The stress distribution is shown in Fig. 1(a). The principle stresses along the silicon beam under a 3 N downward force are displayed in Fig. 3. The center stress on the surface of the beam between the two inner supports is even and uniaxial (mainly in the x axis). The stress distribution along the y and z directions are negligible compared to the stress in the x plane. How the potential changes for voltage input across the resistor is shown in Fig. 4.

5.1. Validation

Ref. [12] presented experimental measurements for a very simple silicon beam under 4PB which is used to validate our results. Also, Ref. [19] used finite element analysis and obtained the numerical results of relative resistance change. Fig. 6 shows the comparison between the three sets of results for silicon beam under piezoresistor's doping concentration of $1 \times 10^{19} \mathrm{cm}^{-3}$. The variation of the relative change of resistance with force is illustrated. A good agreement is found between the present predictions and experimental measurements [12].

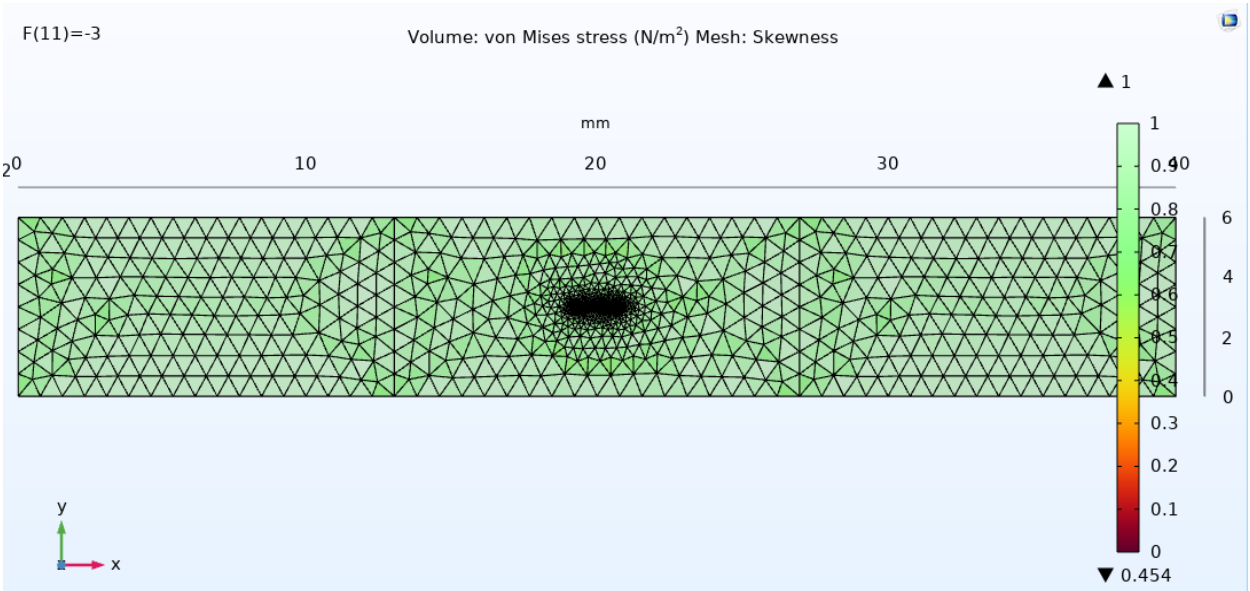

(a)

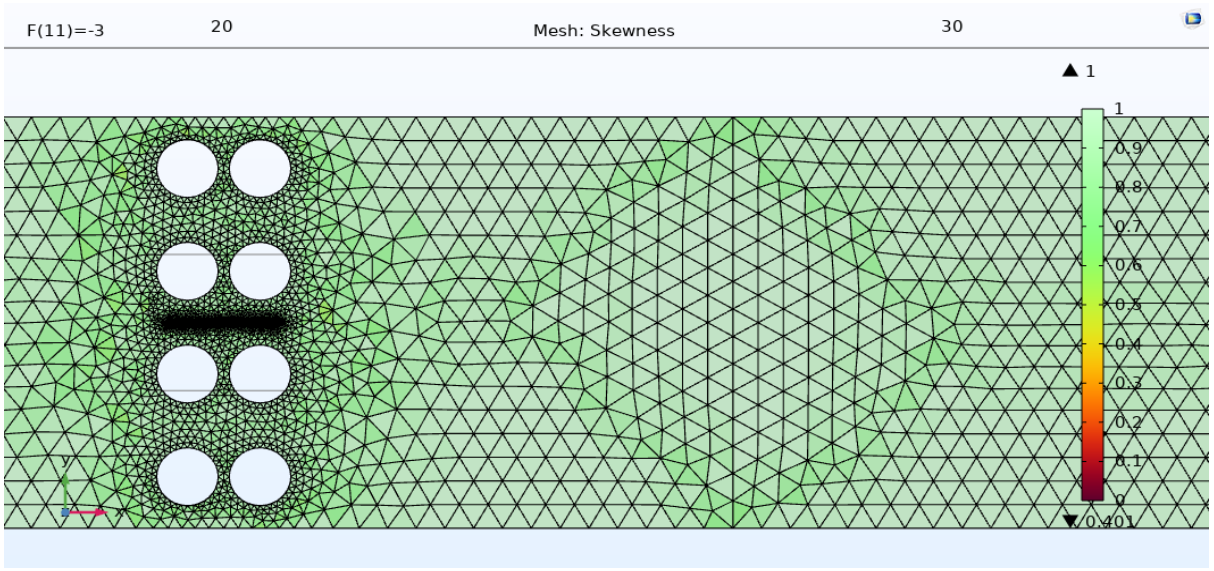

(b)

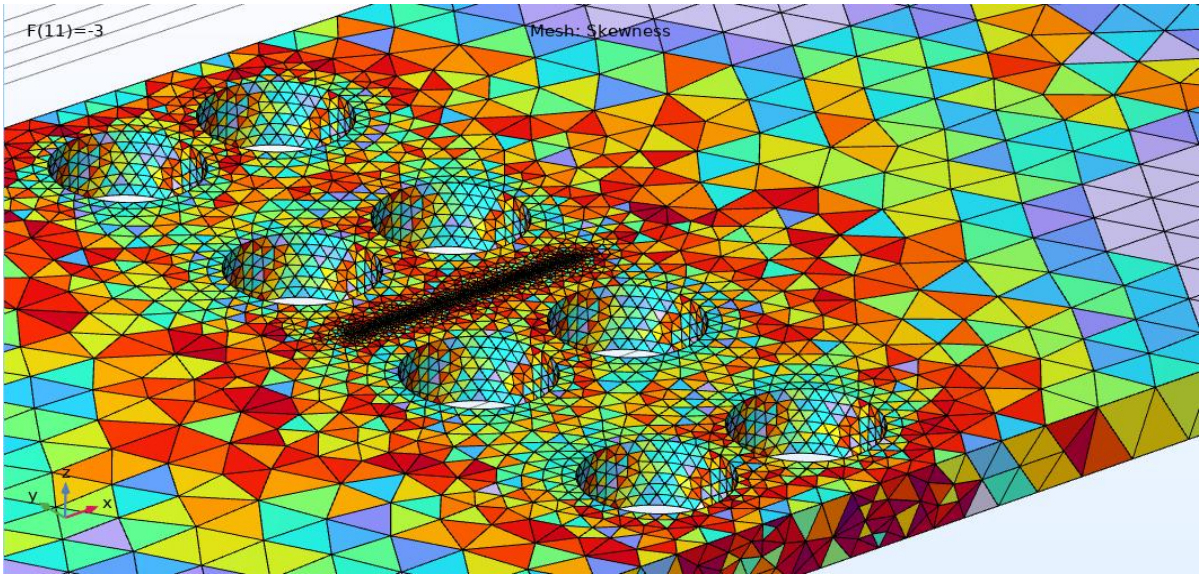

(c)

Fig. 5. Meshing of a silicon beam (a) without SCR and (b) four circular shape SCR (top surface) (c) colored four circular shape SCR side view.

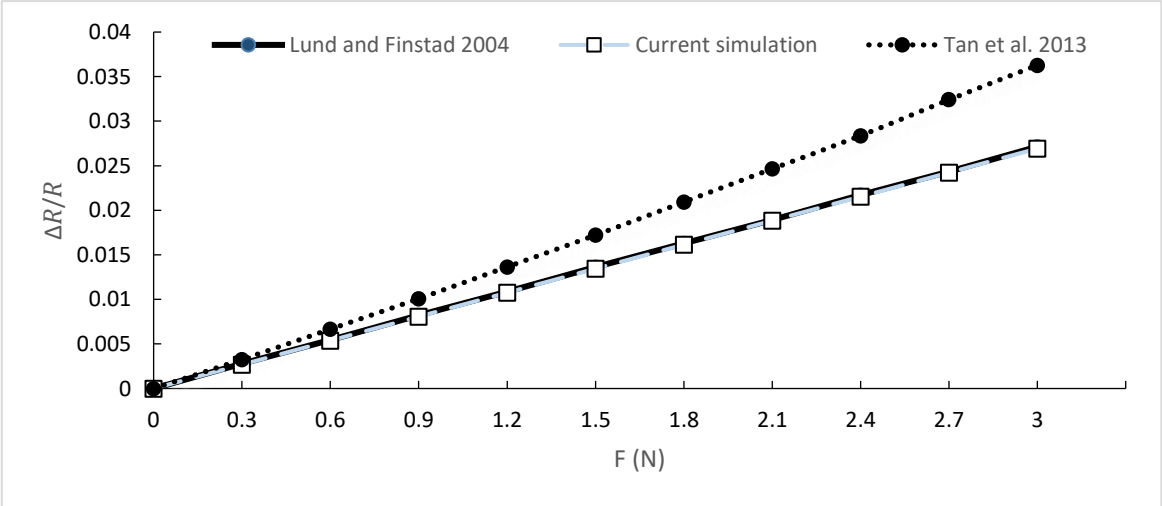

Fig. 6. Comparison between the predictions of current simulation, experimental data [12] and results of Ref. [19]

By using Eqs. (9) and (10) in global evaluation, the relative resistance changes ($\Delta R/R$) are calculated and then compared with the previous literatures.

$$\frac{V}{I} = R \tag{9}$$

$$\frac{\Delta R}{R} = \frac{R_1 - R_0}{R_0} \tag{10}$$

where I and V denote the current and voltage, respectively.

5.2. Mesh Convergence

In the field of finite element analysis, it is a well-established fact that mesh size has great impact on the solution. Irregularly shaped structures, such as triangles or circles, can benefit significantly from a finer mesh. The refinement of the mesh improves the aspect ratio, which is the ratio of the longest edge length to the shortest edge length of the element. This improvement in the aspect ratio helps in reducing the distortion of the elements.

In this section, we utilized a beam with four circles to converge the results. This decision was driven by two primary reasons. Firstly, circular shapes are more sensitive to the mesh due to their unique shape. Secondly, the area of the circles is smaller than that of one and two circles. It is also important to note that around piezoresistor geometry, the mesh size must be finer. This is because the accurate modeling of boundary conditions and contact areas around piezoresistor elements are critical. A fine mesh aids in accurately representing these regions, thereby preventing unrealistic stress concentrations or displacement errors. This, in turn, helps in avoiding incorrect electrical sensitivity responses. Figure 5 shows the mesh density distribution on the upper surface of the silicon beam.

In the process of our modeling, we opted for tetrahedral quadratic elements. This decision was driven by the specific requirements of our model. We employed two different mesh sizes, each tailored to a specific component of our model. For the piezoresistor, we used a mesh with a maximum element size of 0.8 mm and a minimum element size of 0.008 mm. We also incorporated a curvature factor of 0.2. This specific configuration was chosen to accurately capture the geometric intricacies of the piezoresistor and ensure a high level of precision in our results. Fig. 5b provides a visual representation of the mesh density in silicon beam with four circles. For the silicon beam structure, we used a different mesh size. The maximum element size for this component was 3.2 mm, while the minimum was 0.15 mm. We also used a curvature factor of 0.3 for the silicon beam structure.

By carefully selecting these parameters, we were able to achieve convergence in our results. Fig. 7 illustrates the relationship between the size of the elements and the relative resistance change. The simulation began with a coarser mesh, where the maximum element size was 7.2 mm and the number of elements was 56737. As the study progressed, the mesh was gradually refined, and the size of the elements was reduced. The process concluded with an extremely fine mesh with 142640 elements, where the maximum element size was reduced to 1.8 mm.

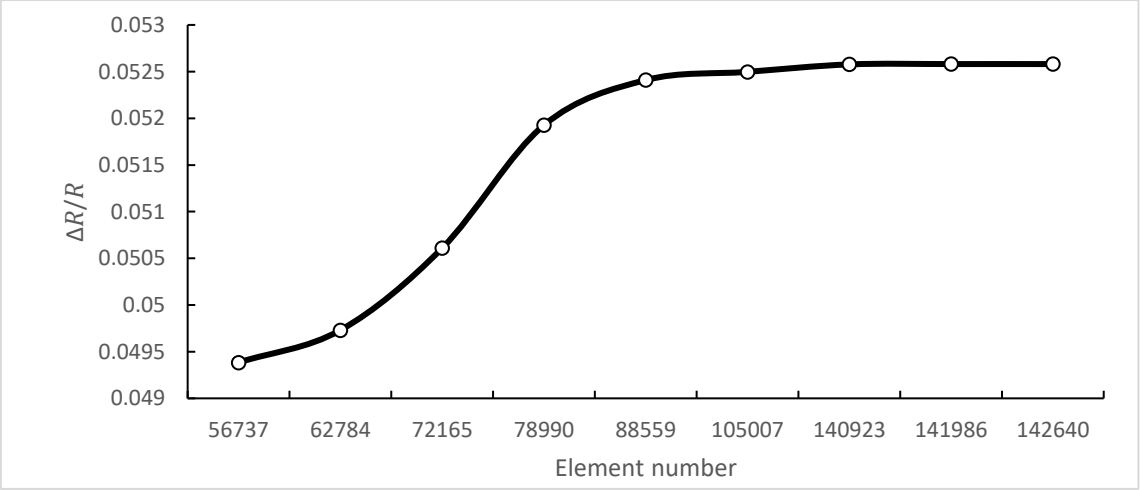

Fig. 7. Mesh sensitivity analysis of relative resistance change by refining mesh sizes.

5.3. Numerical results

Fig. 8 illustrates the variation of relative resistance change with force for different geometrical shapes of SCRs. The structure with hexagonal SCR array shows the maximum resistance change. Thus, the silicon beam with a hexagonal SCR is better effective shape for generating and transferring stress to the piezoresistive sensing mechanism. It shows the highest relative resistance change of 0.057, which is approximately 112% greater than the silicon beam without the SCR. Meanwhile, the relative resistance changes for silicon beams with rectangular, triangular, square, and circular SCR shapes have increased by approximately 48.3%, 60.8%, 95.3%, and 104.5% respectively.

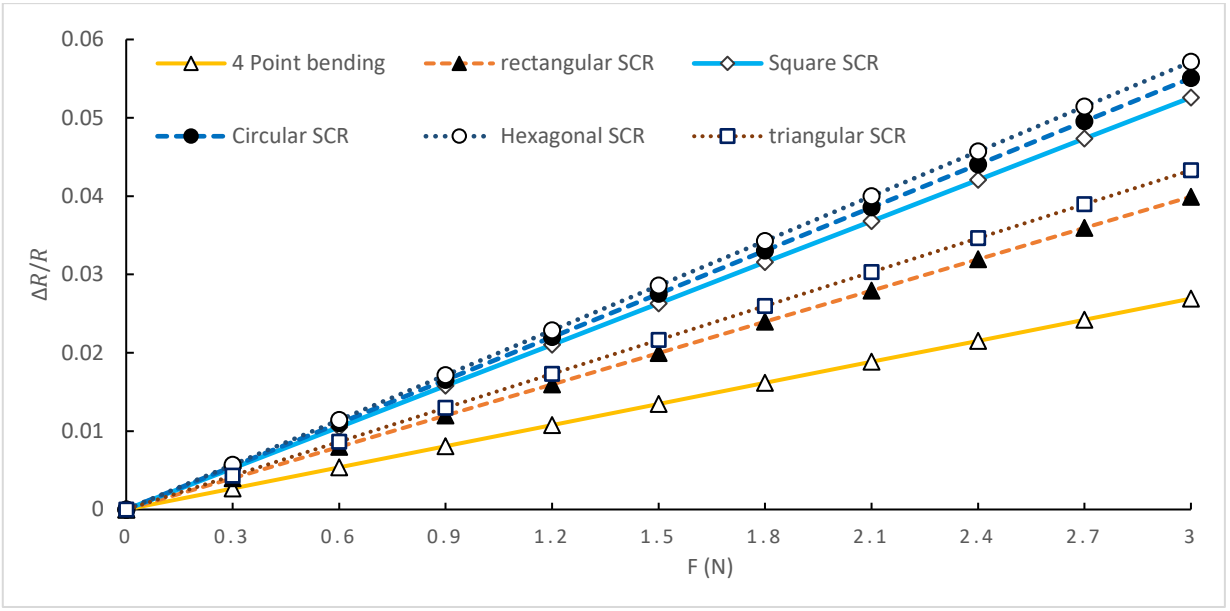

Fig. 8. Correlation between the relative change in resistance (ΔR/R) and the applied force (N) between different SCR shapes.

We also investigated how the results were affected by altering the proximity of the SCRs to the piezoresistor. This involved both bringing the SCRs closer to the resistor and distancing them, and observing the resultant changes. Fig. 9(a-d) illustrate the correlation between the relative resistance change and the applied force for different shapes - square, circular, hexagonal, and triangular - when the distance between the SCRs and the piezoresistor is varied. It is evident from the Fig. 9 that the relative resistivity change exhibits significant variations. This is primarily due to the fact that as the SCRs are moved closer to the piezoresistors, the area of maximum stress shifts closer to the piezoresistors. Consequently, the piezoresistive material exhibits a higher resistivity. In Fig. 9(a) representing the square SCR, it is observed when the SCR is positioned 1mm away from the piezoresistor, the relative resistance change is approximately 35.4% higher compared to the state where the square SCR is positioned in the middle, 1.5 mm from resistor. Conversely, when the SCR is placed 2mm away, there is an 11% decrease in the relative resistivity. A similar trend is observed for other shapes of SCRs under study, with significant changes in the resistivity observed when their distances are altered. For instance, in Fig. 9(b) containing the circular SCR, the closer SCR exhibits an 84% increase in resistivity compared to the middle SCR. However, when the SCR is positioned further away, there is a 14.7% decrease in the relative resistance. In the case of the hexagonal shaped SCR, represented in Fig. 9(c), the closer SCR exhibits a substantial 136.6% increase in relative resistivity change, while the further SCR shows a 13.6% decrease. Finally, Fig. 9(d) presents the results for the triangular shaped SCR. Here, the closer SCR shows a 49% increase in resistivity, while the further one shows a 12.9% decrease in the relative resistivity change. This clearly demonstrates the significant impact of the distance of the SCR from the piezoresistor on the relative resistivity change.

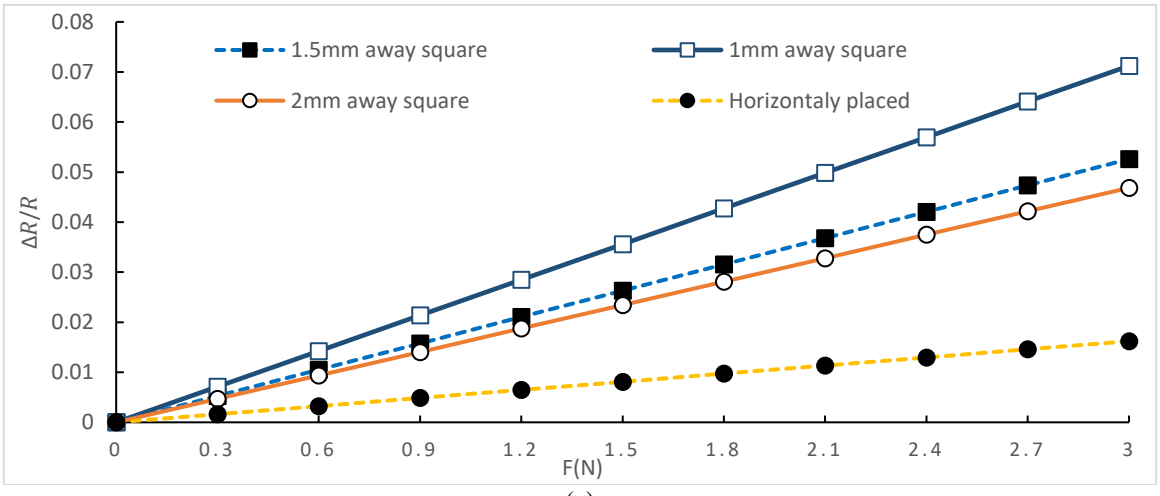

(a)

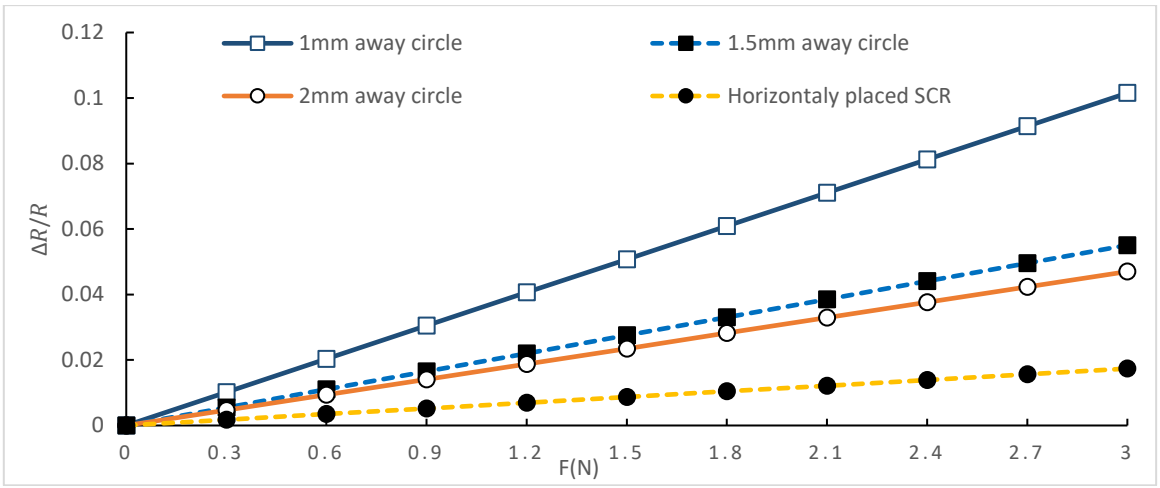

(b)

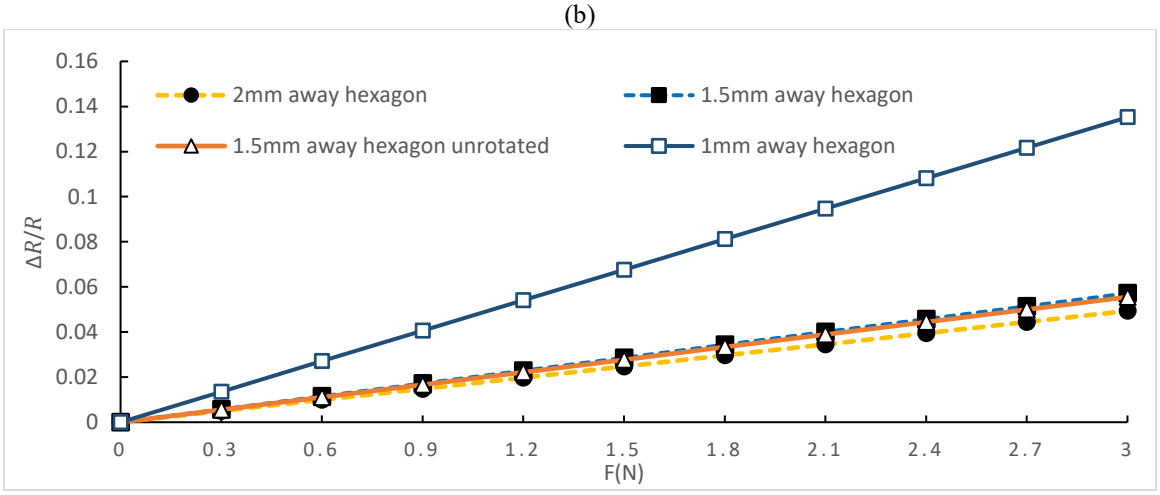

(c)

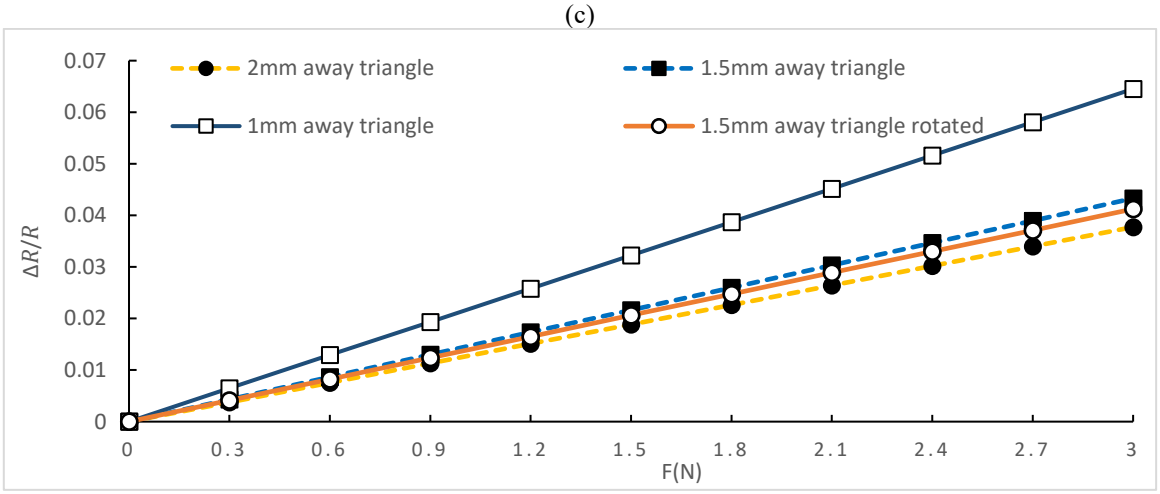

(d)

Fig. 9. Correlation between the *ΔR/R* and the applied force for variation of proximity for (a) square SCR, (b) circular SCR, (c) hexagonal SCR, and (d) triangular SCR

We also conducted a simulation where we rotated angular shapes to observe the impact on the relative resistance. The results of rotating the square SCR at various angles while maintaining the same position are depicted in Fig. 10(a). It is evident from the data that the square SCR, when rotated at an angle of 45°, exhibits the most significant change in the relative resistivity. This is followed by rotations at 30° and 60°, which yield almost identical results. Next in line is the square SCR rotated at 15°, and finally, the unrotated square SCR. The respective increases in resistivity for these configurations are 31.1%, 22.5%, 22%, and 6.9%. From these results, it can be unequivocally inferred that rotating the square SCR enhances the results. This conclusion is supported by the observed increase in resistivity with rotation, which definitively indicates an improvement in performance. Fig.

10(b) shows the results of rotating the triangular SCR at various angles while maintaining the same position. The main positioning, as illustrated in Fig. 1(e) demonstrated the most substantial relative resistance change. On the other hand, when the SCRs underwent rotation, a decline in the results was observed. We conducted a simulation of triangles that were rotated at 30° in both identical and opposite directions, as well as a rotation of 60°. The outcomes were very close to each other, with the triangle rotated at 60° displaying a slightly superior result, showing an approximate decrease of 5%. Additionally, we studied hexagonal-shaped SCRs with different rotations as illustrated in Fig. 10(c). The position we utilized for this shape, as shown in Fig. 1(d), indicated marginally highest changes in relative resistivity, although the overall results remained fairly consistent. For this specific shape, we considered rotations of 15° in both the same and opposite directions, as well as a 30° rotation. For the rectangular SCR, as depicted in Fig. 10(d), this type of SCR exhibited a significant alteration in results. We considered rotations of 15°, 30°, 45°, 60°, and 90°. We also took into account the same and opposite directions for the 45° rotation. The results showed increases of 7.8%, 32.7%, 76.2%, 86.1%, and 161.8%, respectively, in comparison with the main position shown in Fig. 1(f). It is abundantly clear that the rotation of the rectangular shape has a substantial impact on the results. This is likely due to its unique shape and larger size on one side. Moreover, altering the direction of rotation in two rectangles can result in a notable change in outcomes. Also, Fig. 11 illustrates the design and the stress distribution for angular SCR shapes that have been rotated, indicating how the orientation affects the stress distribution within the structure.

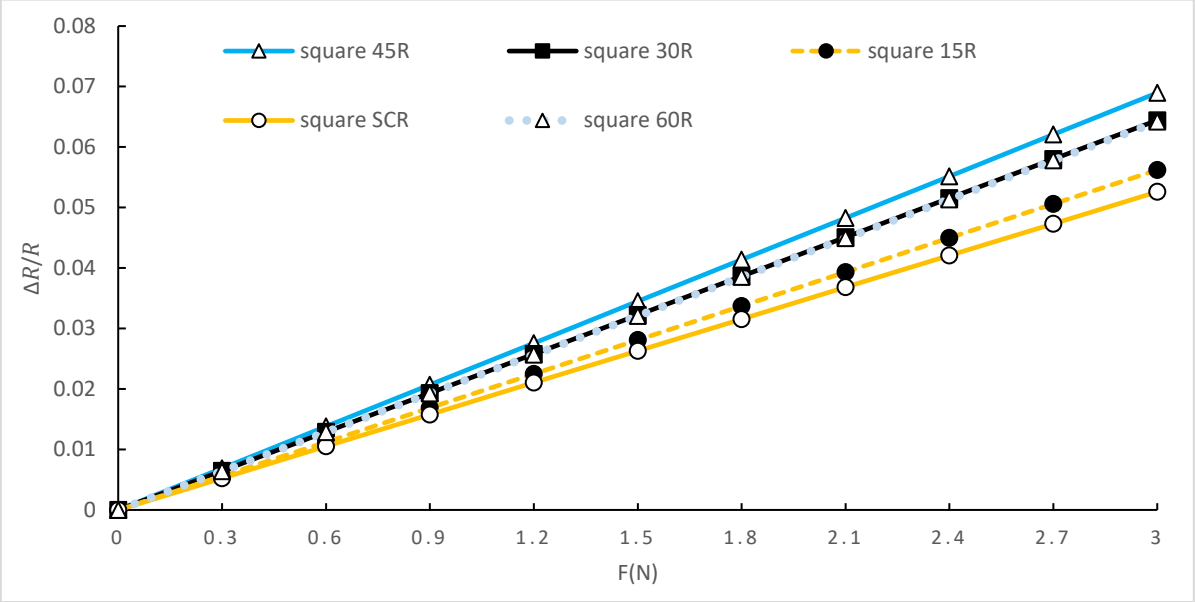

(a)

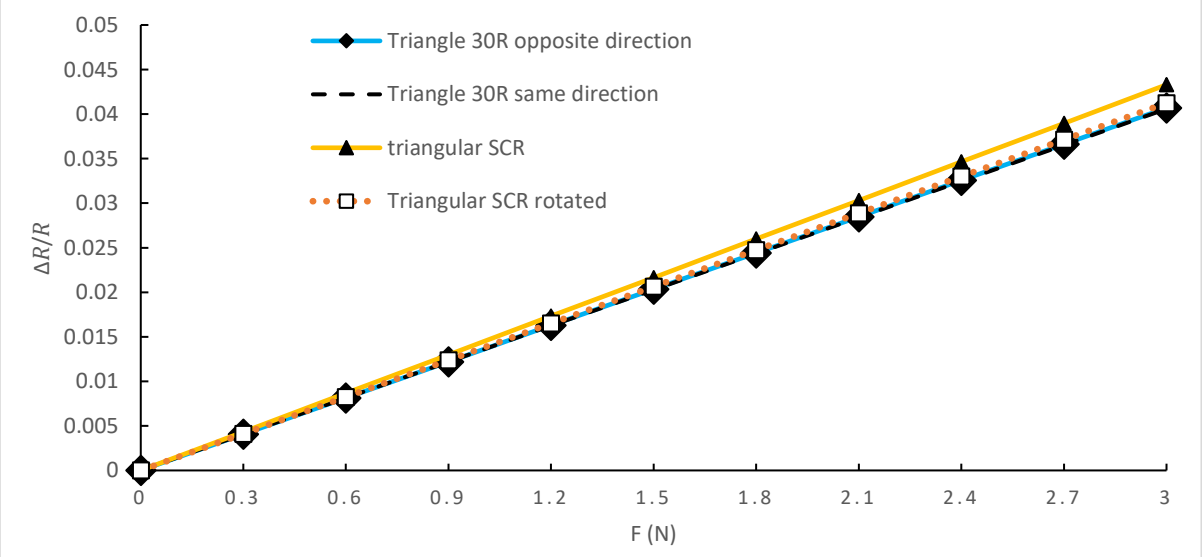

(b)

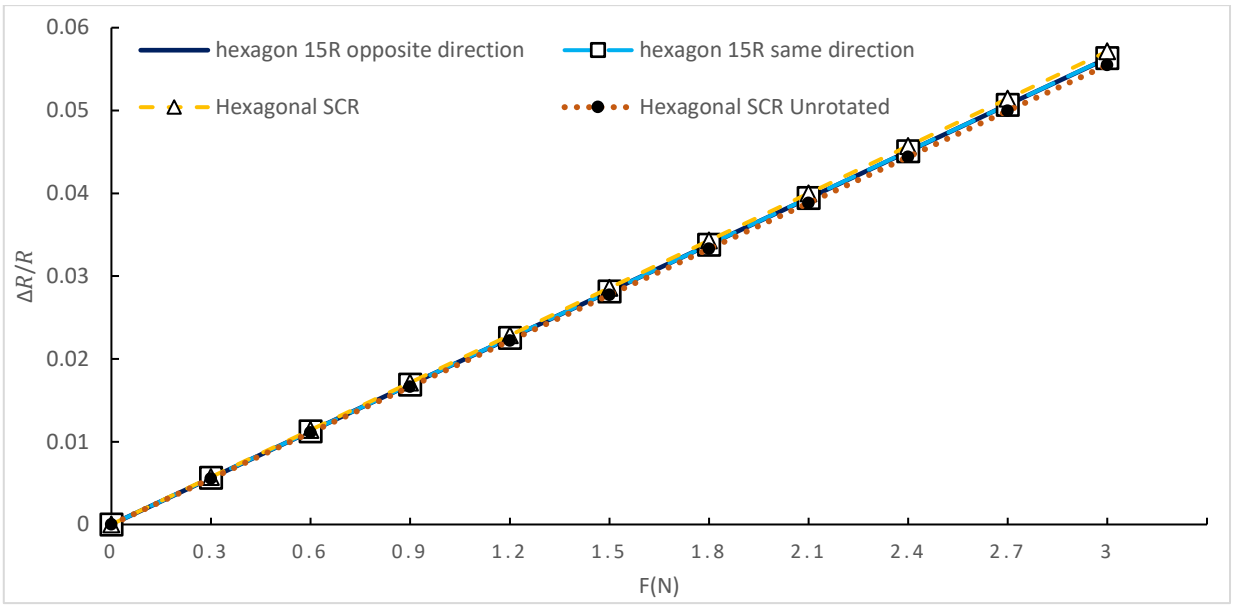

(c)

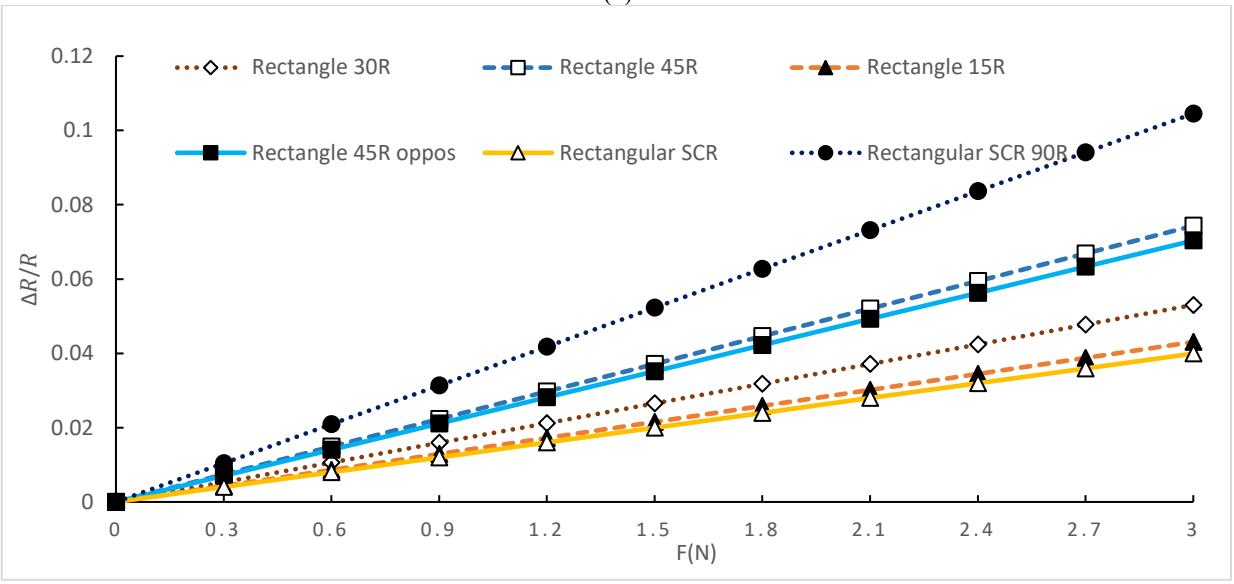

(d)

Fig. 10. Correlation between the *ΔR/R* and the applied force for variation of rotations for (a) square SCR, (b) triangular SCR, (c) hexagonal SCR and (d) rectangular SCR

*R means rotation (for example square 45R means square SCR with 45° rotation)

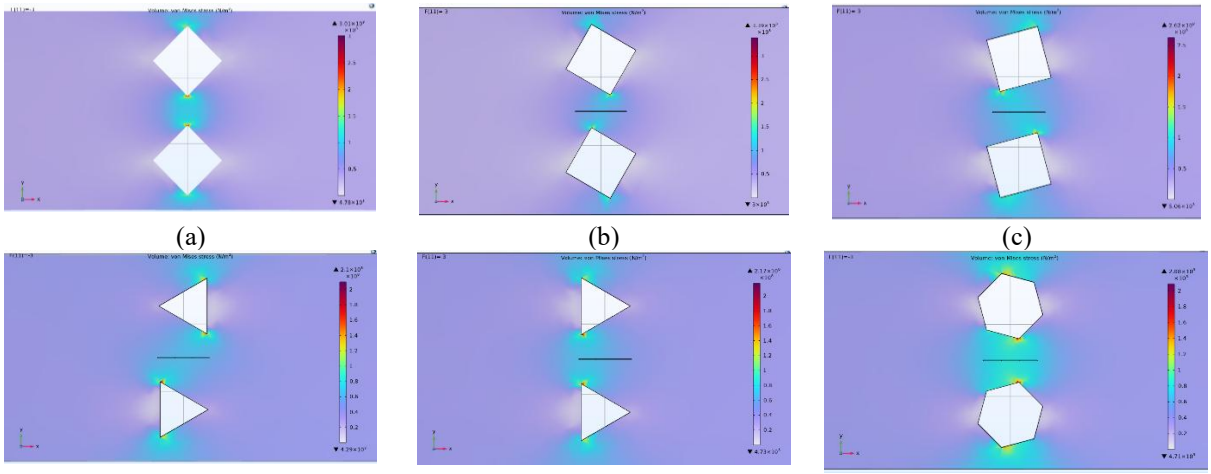

(a) (b) (c)

(d) (e) (f)

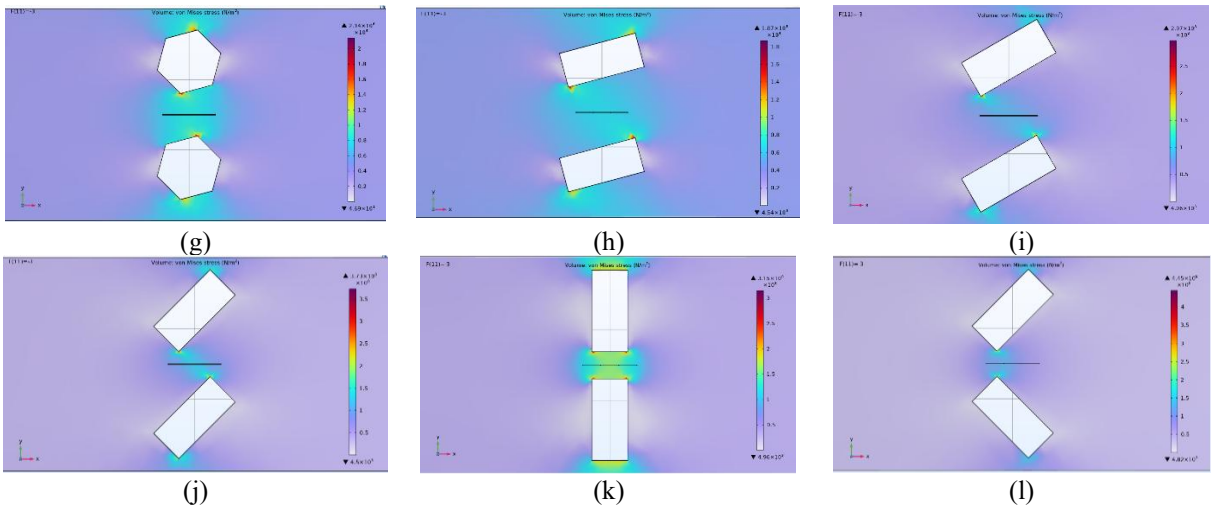

Fig. 11. Design and stress distribution of the rotated angular SCR shapes. (a) 45°, (b) 60° and (c) 30° rotated square (d) 30° rotated in opposite and (e) 30° rotated in the same direction triangles (f) 15° rotated in opposite and (g) 15° rotated in the same direction hexagonal shapes. (h) 15°, (i) 30°, (j) 45°, (k) 90° and (l) 45° opposite rotated rectangular SCRs.

We increased the number of SCRs while maintaining a constant total area for the shapes, which was 2.25 mm^2. For instance, we used four squares each with an area of 0.5625 mm^2, which collectively added up to the total area of 2.25 mm^2. This allowed us to observe the effects of increasing the number of SCRs while keeping the total area constant. For the two SCR shapes, we positioned them vertically to the resistor, which also brought the minimized shapes closer to the resistor. The results related to the increase of number of SCRs are presented in Fig. 12. It is evident that the silicon beam with two circular shapes exhibits the highest relative resistance change, with an increase of 318.7%. Following this is the beam with a hexagonal SCR, both unrotated and rotated, which showed increases of 291.1% and 270.3%, respectively.

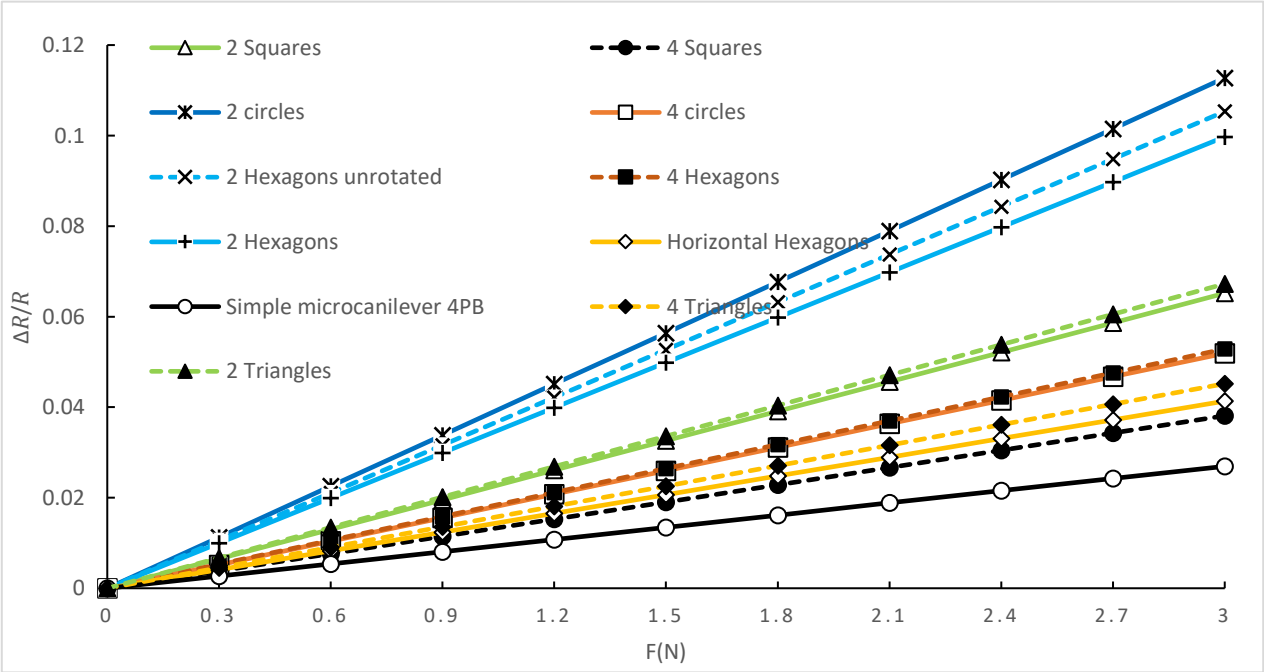

Fig. 12. Correlation between the $\Delta R/R$ and the applied force between various SCR arrays and arrangements.

To emphasize the novelty and importance of the present work, Table 4 compares our findings with relevant studies from the literature. Previous research [13,24,26,31,32,33] has demonstrated that introducing SCRs can enhance piezoresistive sensitivity; however, these works focused on limited geometries or qualitative comparisons. In contrast, the present study provides a systematic FEM-based investigation across multiple SCR shapes, orientations, and distances.

Table 4
Comparison of present work with selected literature

Study (year)	Device / Approach	SCR Type / Method	Reported Sensitivity Change (ΔR/R or qualitative)	Key Notes / source
This work (present)	FEM simulation of p-type Si beam under 4PB loading, systematic SCR analysis	Circular, hexagonal, square, rectangular, triangular (varied distance, rotation, number)	Up to 318.7% increase with dual circular SCRs; ~112% with hexagonal SCR; hexagon performs best; closer SCR → higher ΔR/R	Comprehensive parametric study; identifies best geometry and placement for enhanced piezoresistive response
Bhatti et al. (2007)	FEM of piezoresistive paddle type cantilever with SCR	square holes near fixed end	~33% sensitivity enhancement vs plain cantilever without	Demonstration of SCR benefits through geometric stress concentration holes [24]
Ansari et al. (2013)	Piezoresistive microcantilever biosensor	Triangular, square, and circular SCR designs	Up to 60% improvement in sensitivity compared by implementing SCR to standard beam	Demonstrated practical design of SCRs in biosensors and validated FEM results experimentally [26]
Mondal et al. (2018)	FEM and theoretical modeling of piezoresistive microcantilever	Square arrayed holes / slots for stress localization	600% improvement in output sensitivity	Demonstrated effect of stress-concentrating patterns on cantilever response [31]
Naeli (2009)	FEM modeling of cantilevers with SC	Stress-concentrating beams / wires	Noted ΔR/R improvement with concentrated stress regions	Provided theoretical support for SC [32]
Tran et al. (2018)	Pressure sensor membrane with SCRs	Grooves and holes	Increased stress localization, improved output	Demonstrated SCR application in pressure sensors. proposed structure increases the sensor sensitivity and also reduces the nonlinearity error [33]
Richter et al. (2008)	Semiconductor piezoresistance characterization	— (4PB test method)	Uniform uniaxial stress calibration method	Used as validation benchmark for ΔR/R simulation [13]

6. CONCLUSION

In this work, we employed FEM to investigate the piezoresistive effect in p-type silicon for the design of a basic beam under 4PB loads. This investigation took into account the effect of different shapes, distances, rotations, and the number of SCRs. The results revealed the significant role of incorporating SCRs on a beam structure for enhancing the sensitivity. The relative resistance changes of the silicon beam experiences a substantial increase, up to 318.7%, when two circular-shaped SCRs are included on each side of the piezoresistor. Furthermore, a considerable enhancement, up to 112%, can be achieved merely by opting for a hexagonal shape for the SCRs, meaning the hexagonal SCR demonstrated the best performance, yielding the highest relative resistance change and thus the greatest sensitivity. Also, by reducing the distance between the piezoresistor and the SCR, and by rotating them in certain configurations, the results exhibited a significant change. This suggests that the spatial arrangement and orientation of the SCRs and resistor play a crucial role in determining the sensitivity of the silicon beam or microcantilevers. The placement of these SCRs resulted in improvements in the relative resistance change. Therefore, the hexagonal SCR shape placed closest to the sensing region can be identified as the best configuration for enhancing sensor performance. Generally, the study can provide valuable insights for the design and optimization of various beams for enhanced sensitivity.

REFERENCES

[1] He Y, Yu A, Liu X, Wang Y. Micro Electro-Mechanical Systems (MEMS). In: *Handbook of Integrated Circuit Industry*. Singapore: Springer Nature Singapore; 2023. p. 895-911.
[2] Skidmore G, Ellis M, Geisberger A, Tsui K, Saini R, Huang T, et al. Parallel assembly of microsystems using Si micro electro mechanical systems. *Microelectron Eng*. 2003;67:445-52.
[3] Vashist SK, Holthöfer H. Microcantilevers for sensing applications. *Measurement and Control*. 2010;43(3):84-8.

[4] Algamili AS, Khir MHM, Dennis JO, Ahmed AY, Alabsi SS, Ba Hashwan SS, et al. A review of actuation and sensing mechanisms in MEMS-based sensor devices. *Nanoscale Res Lett*. 2021;16:1-21.
[5] Vashist SK. A review of microcantilevers for sensing applications. 2017. doi:10.2240/azojono0115.
[6] Lamba M, Mittal N, Singh K, Chaudhary H. Design analysis of polysilicon piezoresistors PDMS microcantilever based MEMS force sensor. *Int J Mod Phys B*. 2020;34(09):2050072.
[7] Binnig G, Quate CF, Gerber C. Atomic force microscope. *Phys Rev Lett*. 1986;56(9):930.
[8] Smith CS. Piezoresistance effect in germanium and silicon. *Phys Rev*. 1954;94(1):42.
[9] Beer FP, Johnston JER. *Mechanics of Materials*. 2nd ed. New York: McGraw-Hill; 1981. Chapter 8.
[10] Firdaus SM, Omar H, Azid IA. High sensitive piezoresistive cantilever MEMS based sensor by introducing stress concentration region (SCR). In: *Finite Element Analysis—New Trends and Developments*. 2012. p. 225-52.
[11] Kassenge S, Zoval JM, Mather E, Sarkar K, Hodko D, Maity S. Design issue in SOI-based high sensitivity piezoresistive cantilever devices. In: *SPIE Conference on Smart Structures and Materials*; 2002; San Diego, CA.
[12] Lund E, Finstad TG. Design and construction of a four-point bending based set-up for measurement of piezoresistance in semiconductors. *Rev Sci Instrum*. 2004;75(11):4960-6.
[13] Richter J, Arnoldus MB, Hansen O, Thomsen EV. Four-point bending setup for characterization of semiconductor piezoresistance. *Rev Sci Instrum*. 2008;79(4):044703.
[14] Weihnacht V, Brückner W, Schneider CM. Apparatus for thin-film stress measurement with integrated four-point bending equipment: Performance and results on Cu films. *Rev Sci Instrum*. 2000;71(12):4479-82.
[15] Richter J, Hansen O, Larsen AN, Hansen JL, Eriksen GF, Thomsen EV. Piezoresistance of silicon and strained Si0.9Ge0.1. *Sens Actuators A Phys*. 2005;123:388-96.
[16] Bartholomeyczik J, Brugger S, Ruther P, Paul O. Multidimensional CMOS in-plane stress sensor. *IEEE Sens J*. 2005;5(5):872-82.
[17] Beaty RE, Jaeger RC, Suhling JC, Johnson RW, Butler RD. Evaluation of piezoresistive coefficient variation in silicon stress sensors using a four-point bending test fixture. *IEEE Trans Components Hybrids Manuf Technol*. 1992;15(5):904-14.
[18] Wahid KAA, Lee HW, Shazni MA, Azid IA. Investigation on the effect of different design of SCR on the change of resistance in piezoresistive micro cantilever. *Microsyst Technol*. 2014;20:1079-83.
[19] Tan TH, Mitchell SJN, McNeill DW, Wadsworth H, Strahan S. A computational approach for simulating P-type silicon piezoresistor using four point bending setup. *Simulation*. 2013;6:8.
[20] Kanda Y. A graphical representation of the piezoresistance coefficients in silicon. *IEEE Trans Electron Devices*. 1982;29(1):64-70.
[21] Wortman JJ, Evans RA. Young's modulus, shear modulus, and Poisson's ratio in silicon and germanium. *J Appl Phys*. 1965;36(1):153-6.
[22] Leu PW, Svizhenko A, Cho K. Ab initio calculations of the mechanical and electronic properties of strained Si nanowires. *Phys Rev B*. 2008;77(23):235305.
[23] Noel JG. Review of the properties of gold material for MEMS membrane applications. *IET Circuits Devices Syst*. 2016;10(2):156-61.
[24] Bhatti M, Lee X, Zhong L, Abdalla A. Design and finite element analysis of piezoresistive cantilever with stress concentration holes. In: *ICIEA 2007 - Second IEEE Conference on Industrial Electronics and Applications*; 2007. p. 1171-4.
[25] Kavitha K, Shanmugaraja P, Shree RB. Design and displacement analysis of three different cantilever based MEMS piezoresistive pressure sensor with polymer (PDMS/PMMA) thin film. *Revista GEINTEC*. 2021;11(2):1629-40.
[26] Ansari MZ, Cho C, Choi W, Lee M, Lee S, Kim J. Improving sensitivity of piezoresistive microcantilever biosensors using stress concentration region designs. *J Phys D Appl Phys*. 2013;46(50):505501.
[27] Dhonkal AK, Agarwal V, Sengar K. Sensitivity of the MEMS based piezoresistive wind speed sensor with comparative study of different shapes of paddles. *Int Res J Eng Technol*. 2017;4(2):1693-7.
[28] Rotake DR, Darji AD. Stiffness and sensitivity analysis of microcantilever based piezoresistive sensor for bio-MEMS application. In: *2018 IEEE Sensors*; 2018. p. 1-4.
[29] Hawari HF, Wahab Y, Azmi MT, Shakaff AM, Hashim U, Johari S. Design and analysis of various microcantilever shapes for MEMS based sensing. *J Phys Conf Ser*. 2014;495(1):012045.
[30] Liu Q, Gao R, Tam VW, Li W, Xiao J. Strain monitoring for a bending concrete beam using piezoresistive cement-based sensors. *Constr Build Mater*. 2018;167:338-47.
[31] Mondal S, Arya D, Ansari MZ. High sensitive MEMS piezoresistive microcantilever sensor. *Procedia Comput Sci*. 2018;133:793-8.
[32] Naeli K. *Optimization of piezoresistive cantilevers for static and dynamic sensing applications* [dissertation]. Georgia Institute of Technology; 2009.
[33] Tran AV, Zhang X, Zhu B. Mechanical structural design of a piezoresistive pressure sensor for low-pressure measurement: Computational analysis by increases in sensor sensitivity. *Sensors*. 2018;18(7):2023.